Energy dependence of processing and breakdown properties of Cu and Mo

H. Timko,* M. Aicheler, P. Alknes, S. Calatroni, A. Oltedal,† A. Toerklep, M. Taborelli, and W. Wuensch
CERN, Genève 23, CH-1211, Switzerland

F. Djurabekova and K. Nordlund
Helsinki Institute of Physics and Department of Physics, University of Helsinki, P.O. Box 43, FIN-00014, Finland
(Received 5 April 2011; published 27 October 2011)

Obtaining basic knowledge of breakdowns is desirable in many fields of physics; however, often the energy absorbed by a breakdown is not known or can vary by large amounts. We have therefore investigated how processing and breakdown properties scale with available energy for two materials, Cu and Mo, in the energy range of about 1 mJ to 1 J. A central result obtained is that there appears to be an optimum energy for processing and thus the highest possible electric field a processed material can sustain without breaking down depends on energy accordingly; what this implies for radio frequency cavity processing is discussed as well. For Cu, both the local field and the field enhancement factor showed only a weak dependence on energy; the average of the local field over the entire energy range investigated was (9.6 ± 0.4) GV/m at breakdown. For Mo, the local field increased with increasing energy, while the field enhancement factor remained constant at 34 ± 2. Finally, a possible explanation of the direct current (DC) processing mechanism—at least in the case of Mo—as an oxide removal process is presented.

DOI: 10.1103/PhysRevSTAB.14.101003 PACS numbers: 52.80.Vp, 68.37.Hk

I. INTRODUCTION

In several fields of physics, it is of interest to gain a deeper understanding of electrical breakdowns in vacuum that occur amongst others in fusion devices [1], satellite systems [2], and future linear collider designs [3,4]. The Compact Linear Collider (CLIC) study at CERN is one of these future linear collider designs, demanding a high accelerating gradient to be feasible. Many components, especially the radio frequency (rf) accelerating cavities, must therefore withstand high surface electric fields that provoke electrical breakdowns in ultrahigh vacuum (UHV). A low breakdown probability in the cavities is a key issue for the efficiency of the machine, and thus, basic breakdown studies are indispensable. To complement rf breakdown studies, two direct current (DC) setups are utilized at CERN, which allow for the investigation of breakdown properties in a simple and fast way.

Several materials have already been tested with this DC setup under the same conditions and a ranking of materials according to their ''resistance to breakdown'' has been established [5,6]. In all these earlier DC studies, the energy *available* for a discharge was always about the same, corresponding to the energy contained in a typical CLIC rf pulse. However, the energy *consumed* by a discharge is somewhat less since part of the energy is dissipated by external circuit elements; determining this consumption is nontrivial as discharge buildup is very fast. In rf, on the other hand, the overall energy absorbed during a discharge event can be very precisely determined through incident, transmitted, and reflected pulses; only it is not known how much of this overall absorbed energy is consumed locally by the discharge and how much of it dissipates somewhere else in the cavity, e.g., through breakdown currents.

What is known, however, is that rf pulse energy has an impact on cavity performance and breakdown behavior in many ways. One way to vary rf pulse energy is to vary the pulse length τ; by doing so, the accelerating gradient E that can be achieved while keeping the breakdown probability constant goes down as $E \sim \tau^{-1/6}$ [7,8]. On the other hand, power flow alone does not seem to explain and predict cavity performance satisfyingly; it requires a certain combination of the real (active) and imaginary (reactive) parts of power flow, the so-called ''modified Poynting vector'' [8], to explain performance. Also, it is known that the pulsed heating of the cavity surface caused by the rf magnetic field has a strong influence on breakdown probability and therefore cavity performance [9]. In addition, in tests at the Next Linear Collider Test Accelerator, longer, higher group velocity traveling wave cavities achieved a lower accelerating gradient and received a bigger phase shift during processing. It was suggested that the degraded performance of these cavities is due to more energy being

*Also at Helsinki Institute of Physics and Department of Physics, University of Helsinki, P.O. Box 43, FIN-00014, Finland.
helga.timko@helsinki.fi
†Department of Materials Science and Engineering, Norwegian University of Science and Technology, N-7491 Trondheim, Norway.

absorbed in an individual breakdown [10–12]. Motivated by all these facts whose underlying physics is not yet understood, we have examined with the aid of the DC setup how different material properties scale with the energy available for breakdown.

We will show results for two materials, Cu and Mo, which are the most interesting ones for CLIC and behave in many respects complementary with regard to their breakdown properties. After a detailed description of our measurement methods (Sec. II), we will present for both materials (i) the processing behavior (Sec. III A); (ii) the scaling of breakdown field, field enhancement factor, and local field (Sec. III B) as a function of energy; as well as (iii) the evolution of spot diameter with repeated breakdowns on the same spot (Sec. III C). Finally, we will propose a possible explanation for the processing of materials (Sec. III C) and add concluding remarks (Sec. IV).

II. METHODS

The DC spark setups are described in full detail in [13], we shall highlight here only the essential features of the setups. Figure 1 shows the schematics of the electric circuit used. Discharges are generated between the anode and the cathode under UHV conditions. The anode is a hemispherical tip with a diameter of 2.3 mm; the cathode is a 2 mm thick, rectangular, planar sample (Fig. 2). The electrodes are made of the same material. The electric field required for breakdown is usually of the order of 100 MV/m [6]. Using a 15 kV high voltage power supply, the typical gap spacing d between the electrodes is around 20 μm. As the gap distance is small compared to the radius of the tip, the high electric field is concentrated to a well-defined region where both electrodes can be approximated with two parallel planes, so the external electric field in this region is approximately homogeneous as well. The zero point of the gap distance is measured by the electrodes going into

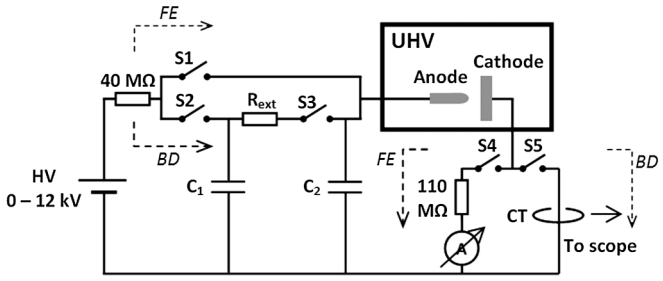

FIG. 1. Schematic drawing of the experimental setup. During field emission measurements (path labeled with "FE"), the switches S1 and S4 are closed. During breakdown field measurements (path labeled with "BD"), first S2 is closed to charge C_1, then switches S3 and S5 are closed, while all other switches are open; thus, the circuit consists of C_1 storing the energy, $R_{\text{ext}} = 25\ \Omega$ limiting the overshoot voltage (and as a consequence, limiting the current during breakdown as well), the overshoot capacitor C_2, and the discharge gap.

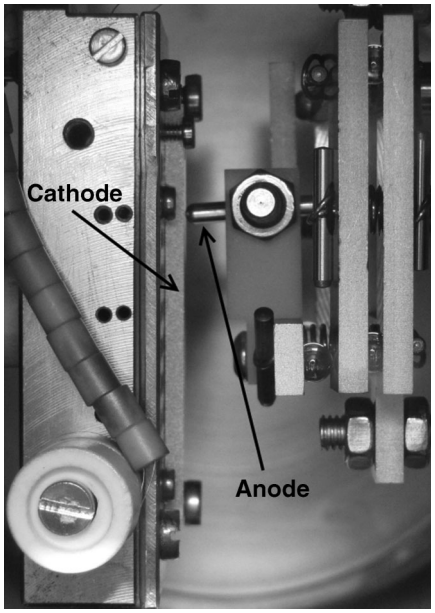

FIG. 2. Picture of the experimental setup. The anode (cylindrical, diameter 2.3 mm, preprocessed) is seen on the right, the cathode (planar) on the left. The typical gap distance is $\approx$ 20 μm. The discharge between the anode and the grounded cathode occurs in ultrahigh vacuum, in the range $\sim 2 \times 10^{-11}$–10^{-9} mbar, in order to match the vacuum conditions required for CLIC.

electric contact; depending on the material, this may slightly modify the electrode surfaces. The desired gap is then obtained by retracting the anode with the aid of a fine adjustment mechanism.

For the results presented here, the field enhancement factor β and the breakdown field E_b have been measured alternately. To determine the *breakdown field*, the voltage V is ramped up stepwise, until a discharge occurs. The breakdown field is then the last value of external electric field before the breakdown. By measuring E_b repeatedly on the same spot, some materials exhibit *conditioning* (e.g., Mo [6]), and some *deconditioning* (e.g., Cu [14]). Conditioning or deconditioning, that is, processing means that after a certain amount of sparks, E_b is higher or lower, respectively, than measured on a virgin surface. Thus, we define the *saturated field* E_{sat} as the average breakdown field reached after the processing phase. This saturated field can be compared to accelerating gradients reached at a given breakdown probability in rf structures by taking into account that the saturated field corresponds to a breakdown probability of about 10^{-2} [6].

The *field enhancement factor* β describes by what factor the external field E_{ext} is enhanced locally at the cathode surface. This enhanced field gives rise to field emission from the cathode and we call it the *local field* $E_{\text{loc}} = \beta E_{\text{ext}}$. E_{loc} cannot be directly measured and is therefore derived from the E_b of a given breakdown and the β measured prior to it. We determine β through a so-called "field

emission scan." During such a scan, the electron field emission current is measured and the corresponding current density j_{FE} is deduced as a function of external field. β is then determined by a least-squares fit to the Fowler-Nordheim (FN) equation [15–18]:

$$j_{\mathrm{FE}}(E_{\mathrm{loc}}) = a_{\mathrm{FN}} \frac{(eE_{\mathrm{loc}})^2}{\phi t(y)^2} \exp\left(-b_{\mathrm{FN}} \frac{\phi^{3/2} v(y)}{eE_{\mathrm{loc}}}\right), \quad (1)$$

where ϕ is the work function and e the elementary charge. The value $\phi = 4.5$ eV [19] has been used as an average both for polycrystalline Cu and Mo. $t(y)$ and $v(y)$ are elliptical integral functions of the variable

$$y = \sqrt{\frac{e^3 E_{\mathrm{loc}}}{4\pi\varepsilon_0 \phi^2}}, \quad (2)$$

where ε_0 is the permittivity of vacuum. The constants a_{FN} and b_{FN} stand for

$$a_{\mathrm{FN}} = \frac{e}{16\pi^2\hbar} = 1.5414 \times 10^{-6} \frac{\mathrm{A}}{\mathrm{eV}},$$
$$b_{\mathrm{FN}} = \frac{4\sqrt{2m_e}}{3\hbar} = 6.8309 \times 10^{9} \frac{1}{\sqrt{\mathrm{eV}}\mathrm{m}}, \quad (3)$$

when $[j_{\mathrm{FN}}] = \mathrm{A/m^2}$, $[E_{\mathrm{loc}}] = \mathrm{V/m}$ and $[\phi] = \mathrm{eV}$, and where $\hbar$ is the reduced Planck constant and m_{e} the electron mass. The Wang and Loew approximation [20] has been used for the elliptic functions $t(y)$ and $v(y)$, setting $t(y) = 1$ and $v(y) = 0.956–1.062y^2$.

To measure the breakdown field, first the main external capacitor C_1 is charged to a given voltage, with the switch S2 closed and other switches open (cf. Fig. 1). When the capacitor is fully charged, the power supply is disconnected by opening S2. Then S3 and S5 are closed for 2 s, during which a breakdown can occur. This time is sufficiently long as breakdowns usually occur during the first few μs-ms [14]. In addition, an overshoot capacitor $C_2 = 0.167$ nF has been used, which is small compared to C_1, that is varied in order to study energy dependence. However, through the presence of C_2, the voltage over the discharge gap will be not exactly the charging voltage, but is influenced by the ratio C_2/C_1. All measurement data presented here take this into account.

Since the main objective of the present paper is to explore the change of breakdown properties as a function of energy available for breakdown, some details regarding this energy have to be pointed out. The energy stored in the external capacitor is $W = \frac{1}{2} C_1 V^2$, where V is the charging voltage over the discharge gap. The external field applied to the discharge gap is $E_{\mathrm{ext}} = V/d$, where d is the gap distance. The energy dependence is probed by changing C_1. However, the correlation between C_1 dependence and energy dependence is not simply linear: Even with a given C_1, the energy available for a breakdown may vary with the breakdown field (and corresponding V) achieved; in addition, the breakdown field itself may depend on W (investigated in Secs. III B 1 and III B 2).

It should be emphasized as well that the energy *available* for a breakdown is not necessarily the same as the energy *consumed* by a breakdown: Part of the energy is dissipated in other circuit elements. Ideally, the energy consumed could be determined by measuring the current-voltage characteristic of the breakdown. At the present, however, the measurement system has resonances in the ~10–100 MHz regime that restrain us from measuring the current-voltage characteristics reliably. Typical current-voltage characteristics in the low and high energy regimes are shown in Fig. 3. Based on the current signal, the total duration of the arc ranges from 0.5 to 2 μs in low and high energy regimes, respectively; corresponding peak currents range from 40–80 A to 100–120 A. Even though a precise measurement of consumed energy is currently not possible with our system that is resonant on the time scale of the discharge, it is reasonable to assume that more energy

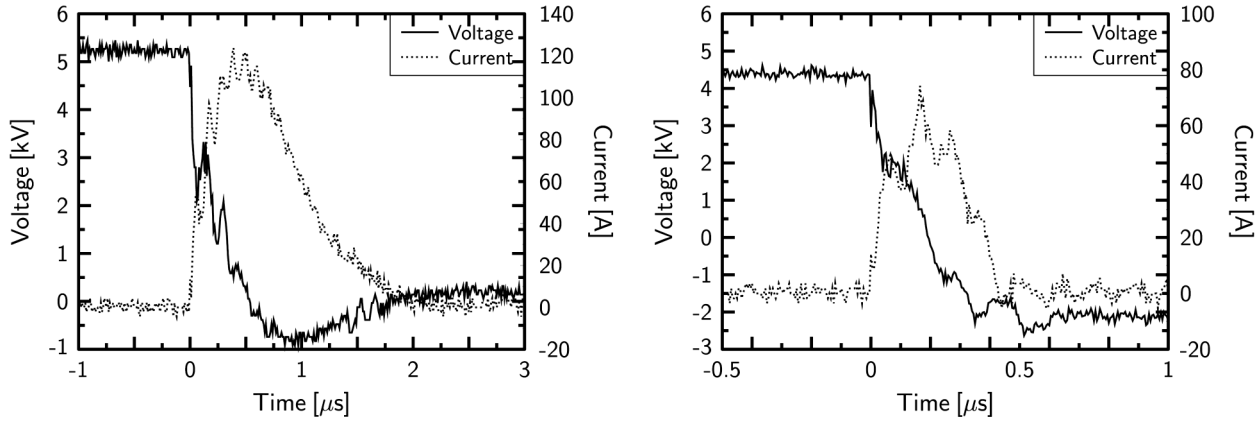

FIG. 3. Typical current-voltage characteristics for different energy regimes. Resonances limit the reliability of the signals. Note that negative voltages are an artifact of the measurement. (a) Cu, $C_1 = 15$ nF. (b) Cu, $C_1 = 2$ nF.

TABLE I. Samples and surface treatments investigated.

Material	Surface treatment	Investigated properties
Cu	As received	Processing (Sec. III A), energy dependence (Sec. III B 1)
	As received	Processing (Sec. III A), energy dependence (Sec. III B 2)
Mo	Electropolished	Spot evolution (Sec. III C)
	Electropolished, heat treated (UHV, 2 h, 1000°C)	Spot evolution (Sec. III C)

available will result in more energy consumed by the arc. The exact dependence between energy available and consumed is yet to be determined, both in DC and rf cases. Thus in this article, given the relevance of results for rf breakdown studies, we present all our data as a function of available energy.

In our measurements, the following capacitances have been used for C_1: 0.56, 2, 15, 27.5, and 60 nF, corresponding to an energy range of about 5 to 240 mJ for Cu and about 10 to 1100 mJ for Mo (in all earlier measurements the ''standard'' capacitance used was 27.5 nF). Lowering the external capacitance further is beyond the means of the present experimental setup, because the external capacitance would start to be comparable with the overall internal system capacitance (which is due to cables, etc.; for further details, see Sec. IV).

The materials tested are Cu (OFE, UNS C10100) and Mo (99.95% purity). All samples were cleaned according to the CERN standard procedure [21]. Several samples with different surface treatments have been prepared. These are summarized in Table I. To study the energy dependence of breakdown properties, only one sample of each material has been used; the sample-to-sample reproducibility of measurements has been demonstrated earlier over many years of testing with the DC setup [5,6]. All tests have been carried out with virgin cathodes, but processed (sparked) anodes.

Concerning error estimates presented in this paper, we note that we have consequently used the standard error instead of the standard deviation to estimate the uncertainty of our data. This choice was motivated by previous measurement results with the DC setup, which have shown that even though E_b varies much in a processing curve, when measuring breakdown probability as a function of electric field (not presented in this paper), a change of about 10–15 MV/m [6,14] translates to an order of magnitude difference in breakdown probability. Since the E_{sat} of a processing curve corresponds to a breakdown probability of about 10^{-2} [6], it is reasonable to assume that we can measure E_{sat} rather accurately. Hence, a more realistic error estimate for E_{sat} is given by the standard error, which takes into account the large amount of statistics collected in a processing curve.

III. RESULTS

A. Processing

The processing behavior of Cu and Mo for high energy sparks ($\sim$ 0.1–1 J) is known from previous measurements [5,6]. Typical processing curves for these cases are shown in Fig. 4. In general, Mo exhibits a long conditioning (30–50 breakdowns), while Cu rather deconditions and does this almost immediately ($\sim$ 2–10 breakdowns). Because of fluctuations, it may sometimes appear as if one could not exclude a very slow conditioning of Cu either [cf. Fig. 5(a)]. However, previous measurements with 300 and more breakdowns per processing curve showed that E_{sat} remains constant, confirming that the processing period of Cu is short [6]. In addition, experiments on thermally oxidized Cu

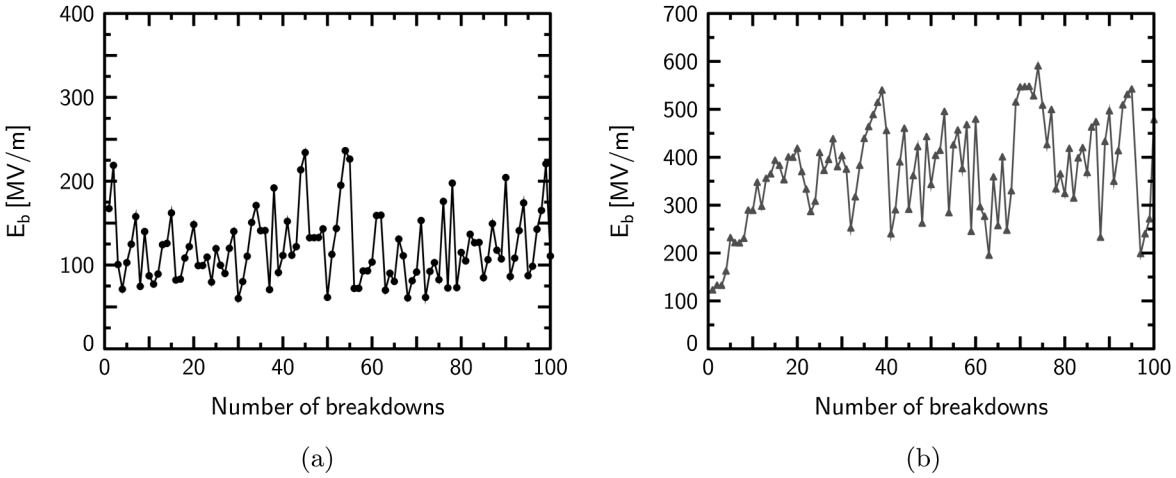

FIG. 4. Typical processing curves measured with $C_1 = 27.5$ nF (corresponding to the order of $\sim$0.1–1 J). E_{sat} is the average of E_b excluding the processing phase, that is, the first 10 sparks for Cu and the first 40 sparks for Mo, and the error is the standard error of the same data points. (a) Cu, $E_{\mathrm{sat}} = (121 \pm 4)$ MV/m. (b) Mo, $E_{\mathrm{sat}} = (403 \pm 9)$ MV/m.

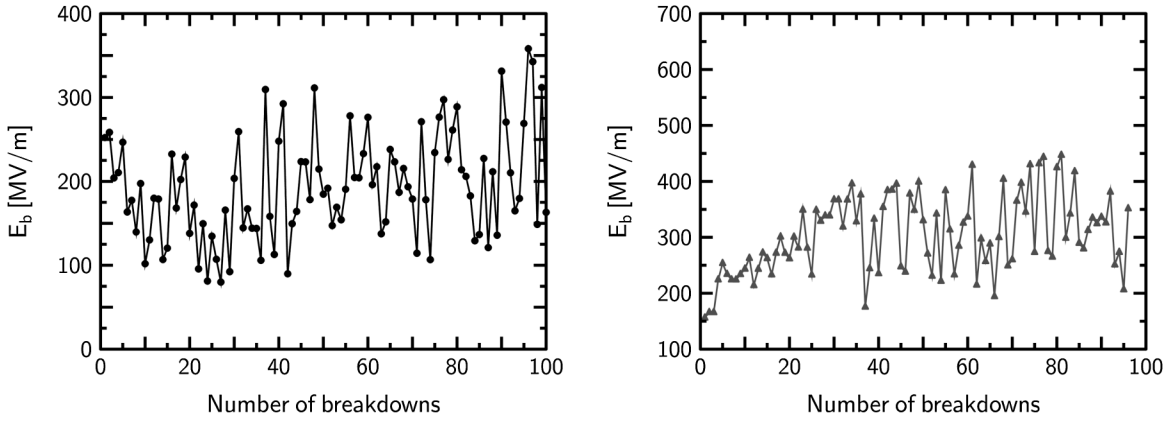

FIG. 5. Processing curves for the lowest capacitance, $C_1 = 0.56$ nF. The length of the processing phase remains the same. Cu always deconditions, while Mo always conditions. E_{sat} is the average of E_b excluding the processing phase, that is, the first 10 sparks for Cu and the first 40 sparks for Mo, and the error is the standard error of the same data points. (a) Cu, $E_{\mathrm{sat}} = (189 \pm 6)$ MV/m. (b) Mo, $E_{\mathrm{sat}} = (324 \pm 9)$ MV/m.

resulted in a longer processing phase (up to 20–30 breakdowns for a $\gtrsim 15$ nm thick oxide layer), showing clearly that Cu deconditions [6]. Concerning the energy dependency of the processing behavior, for both materials the length of the processing phase as well as the tendency of processing (conditioning or deconditioning) remained unchanged at lower energies (see Fig. 5).

To further investigate the processing of Mo, in some cases also *high energy preprocessing* was performed, in analogy to high peak power processing of superconducting cavities [22]. High energy preprocessing means that the processing was performed first with the standard capacitance (27.5 nF) for the first 40 sparks, and then a lower capacitance (2 nF) was used to measure E_{sat}. Performing the usual processing with only the lower capacitance throughout all the processing curve results in $E_{\mathrm{sat}} = (290 \pm 20)$ MV/m. By applying high energy preprocessing a much higher field is reached, $E_{\mathrm{sat}} = (400 \pm 30)$ MV/m. Note that both these values are averages over several independent measurements; the errors represent the accumulated error of the standard error of 2–3 independent measurement series and the average standard error of data points per series. The result indicates that the surface can be conditioned more efficiently if the energy available for breakdown during the processing phase is suitably chosen, which could be most interesting for the often time-consuming processing of rf cavities as well.

B. Scaling of breakdown properties with energy

1. Cu

The breakdown properties (field enhancement factor, saturated, and local field) of Cu as a function of energy are shown in Fig. 6. The diameter of the damaged area (spot) has been studied as well, both as a function of energy and number of sparks. For a typical ~100–200 sparks applied per spot, the dependence of spot diameter with energy is shown in Fig. 6(d). Naturally, the spot size is increasing with increasing energy. Note that, in this range, the spot diameter does *not* depend on the total number of sparks; this will be further discussed in Sec. III C.

The saturated field is seen to decrease with increasing energy [Fig. 6(a)]; however, this tendency might be saturating with the highest capacitance, 60 nF. The decrease in saturated field is attributed to the fact that Cu always deconditions, implying that the higher the energy, the more effective the deconditioning is. With about 90–240 mJ energy available, deconditioning reaches its maximum efficiency within the investigated range.

The dependence of the field enhancement factor [Fig. 6(b)] and the local field [Fig. 6(c)] on energy, if there is any, is very weak, given that an energy range spanning 2 orders of magnitude has been investigated. Both in theory [23] and earlier experiments with $C_1 = 27.5$ nF [14], it has been observed for Cu that one requirement for breakdown to occur is to reach a critical local field of 10–11 GV/m. Calculating now the average of the local field over the entire energy range of Fig. 6(c), we arrive at (9.6 ± 0.4) GV/m. This result suggests that earlier observations of a constant local field for Cu can be extended to the newly investigated energy range, meaning also that if E_{sat} is lower for higher energies, field emitters having higher β would need to be created in order to reach breakdown.

The surface damage caused by breakdowns in the low and high energy regimes has been observed qualitatively with the aid of scanning electron microscopy (SEM), see Figs. 7(a) and 7(b). Only the cathode damage has been investigated, since earlier measurements have shown that breakdown properties depend solely on the material of the cathode and the related cathodic processes [6]. At first glance, deep craters and fingerlike structures originating

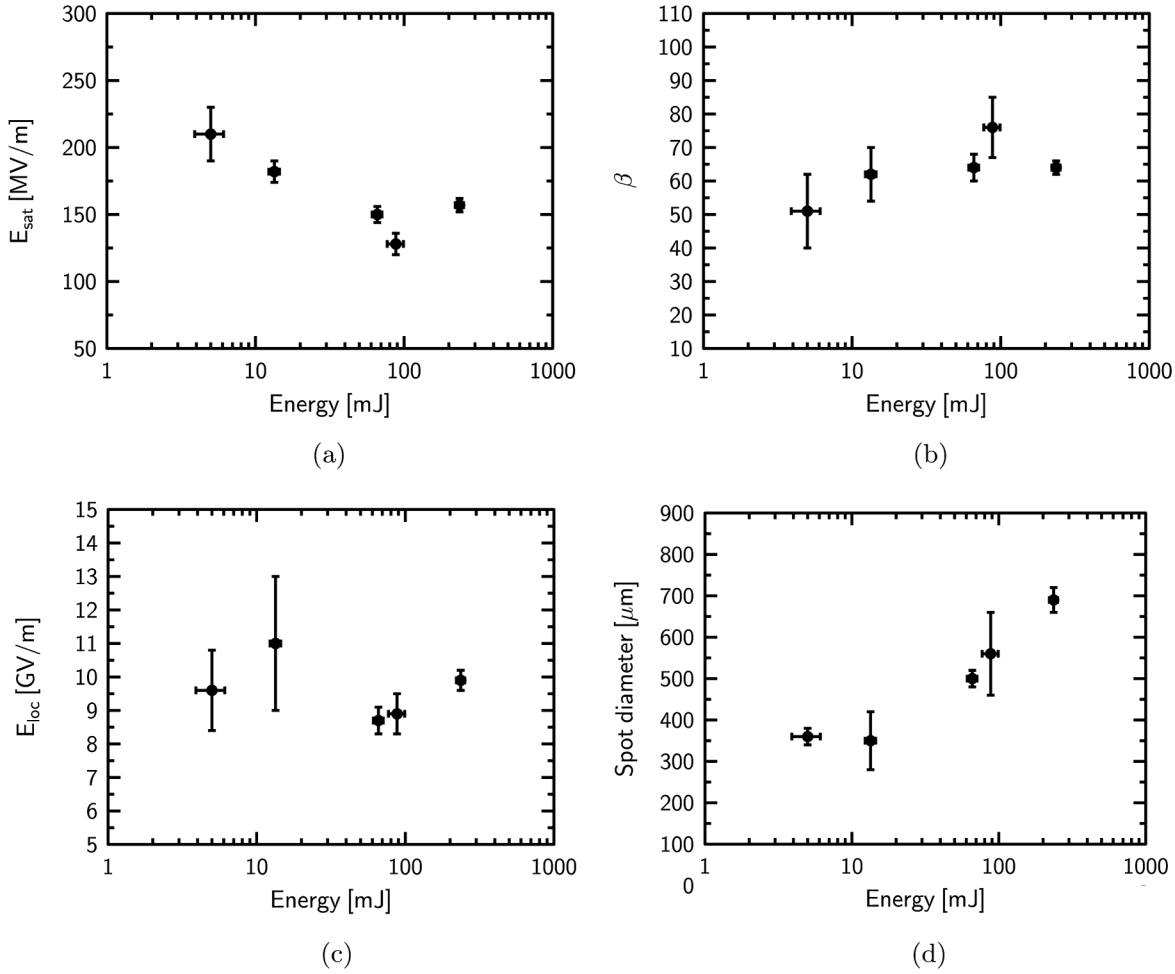

FIG. 6. Breakdown properties of Cu as a function of energy. The energy values correspond to the energy stored in the external capacitor, Ohmic losses on the external circuit components have not been extracted. Each plotted point corresponds to an average of 2–3 measurement series carried out with the same capacitor in processing mode (excluding the processing phase), with up to 250 sparks per series. Vertical errors show the accumulated error of the standard error of the 2–3 series and the average standard error of data points per series. Horizontal errors show the spread in energy due to the uncertainty in saturated field. (a) Saturated field. (b) Field enhancement factor. (c) Local field. (d) Spot diameter.

from large molten droplets (clusters) sputtered from the cathode seem to be exceedingly present for breakdowns produced with the largest capacitances [Fig. 7(b)], suggesting that the more the deposited energy is lowered, the shallower craters are and the less fingerlike structures are seen.

However, in order to compare the surface damage in the low and high energy regimes caused by the same dose per area (particle and energy flux), we have magnified the low energy regime image by a factor of $\sqrt{E_h/E_l}$, where E_h and E_l is the impact energy of high and low energy regime images, respectively. The magnified image [Fig. 7(c)] supports at least visually self-similarity to Fig. 7(b), suggesting that the higher the energy is, the deeper the breakdown-caused surface damage, and as a consequence, the more efficient oxide removal processing would be. A combined atomic force microscopy and SEM observation of low and high energy regime craters would be needed to prove self-similarity also quantitatively.

2. Mo

The same breakdown properties as for Cu have been investigated for Mo as well, with the same capacitances (0.56, 2, 15, 27.5, and 60 nF). Results are shown in Fig. 8. Compared to Cu, the energy range investigated for Mo is somewhat shifted to higher values, which is due to the higher E_{sat} of Mo (and therefore, higher applied voltages).

The spot diameter exhibits a similar scaling with energy as it did in the case of Cu, growing from ~600–1100 μm over the measured energy range. The breakdown-caused surface damage has been observed with SEM also for Mo in the different energy regimes, see Fig. 9; however, the resolution of the analysis was insufficient to compare the damage caused by the same flux.

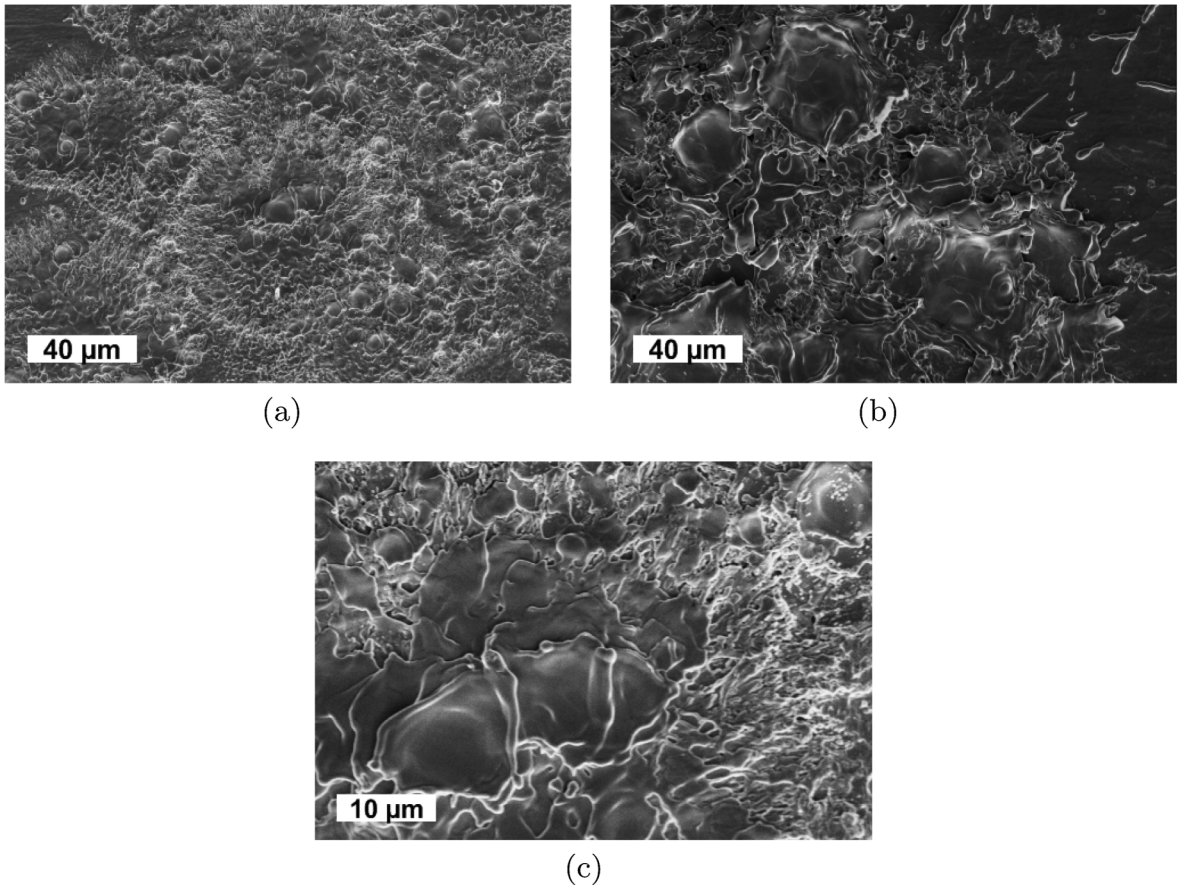

FIG. 7. SEM images of surface damage for Cu for low and high energy regimes. When scaled to the same energy flux, low and high energy regimes exhibit visual self-similarity. (a) Surface damage for $C_1 = 0.56$ nF (~ 5 mJ); the total number of sparks on the spot was 131. (b) Surface damage for $C_1 = 27.5$ nF (~ 90 mJ); the total number of sparks on the spot was 125. (c) Surface damage for $C_1 = 0.56$ nF (~ 5 mJ); magnified by a factor of $\sqrt{90/5} \approx 4$.

The saturated field of Mo [Fig. 8(a)] shows a clear trend of increase with increasing energy, with the increase becoming less clear around 850–1100 mJ. This trend, although being opposite, is analogous to the scaling of the saturated field for Cu, when interpreted in terms of a more efficient processing with more energy available; it suggests that for a particular material and a given breakdown probability there is always an ''optimum energy'' at which the highest possible saturated field in DC or accelerating gradient in rf can be reached. Contrary to Cu, for Mo it is the field enhancement factor [Fig. 8(b)] that can be interpreted as a constant over the energy range investigated. The overall average field enhancement factor is 34 ± 2. Thus, the local field of Mo [Fig. 8(c)] does not remain constant, but follows the same trend as the saturated field does.

As it can be concluded from the presented experimental data on Mo and Cu, the processing behavior and the energy dependence are material dependent. The facts that the material exhibiting deconditioning during processing (Cu) shows a decrease of E_{sat} as a function of energy and that the material exhibiting conditioning (Mo) shows an increase of E_{sat} as a function of energy, indicate a correlation between the processing behavior and the energy dependence of E_{sat}; the E_{sat} that can be reached on a given material would then depend on the energy available for surface processing. A somewhat similar effect in rf technology is that higher group velocity structures require in general more input power, and thus for the same pulse length and breakdown probability the surface fields reached are lower [8,24].

C. Evolution of spot diameter

Since the processing phase seems to play such a central role in how different quantities develop, we took also a closer look at the development of the spot diameter during the processing phase of Mo, which is about 40 sparks. We investigated the damage caused by 1, 5, 10, 20, and 40 sparks, where each spot was created on a new, undamaged area. Another motivation for inspecting spot size evolution more closely was the fact that, in the range of 100–250 sparks, the spot sizes presented in Sec. III B turned out to

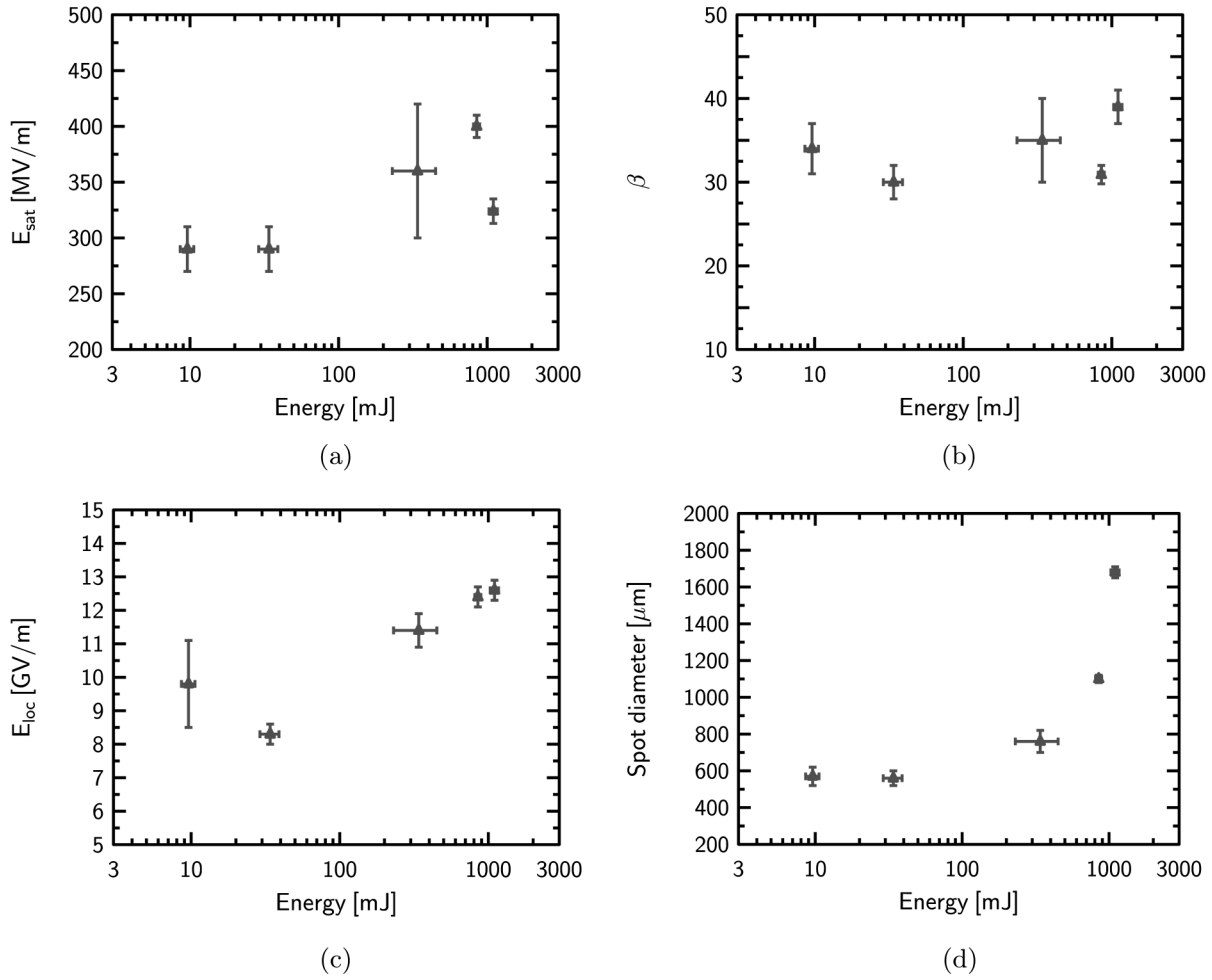

FIG. 8. Breakdown properties of Mo as a function of energy. The energy values correspond to the energy stored in the external capacitor, Ohmic losses on the external circuit components have not been extracted. Each plotted point corresponds to an average of 2–3 measurement series carried out with the same capacitor in processing mode (excluding the processing phase), with up to 250 sparks per series. Vertical errors show the accumulated error of the standard error of the 2–3 series and the average standard error of data points per series. Horizontal errors show the spread in energy due to the uncertainty in saturated field. Note that while the same capacitors were used both for Cu and Mo, the explored energy range lays higher for Mo, because of its higher E_{sat}. (a) Saturated field. (b) Field enhancement factor. (c) Local field. (d) Spot diameter.

be independent of the number of sparks, implying that the final spot sizes would have to develop during the first few sparks of the processing curve.

All measurements were carried out with the standard capacitance, $C_1 = 27.5$ nF. Two Mo samples with different surface treatments—both electropolished and one subsequently heat treated—have been tested (cf. Table I). The heat treatment above 1000°C was known from previous measurements to remove the oxide layer almost fully and reduce the length of the processing phase accordingly [6,25]. This was confirmed also by x-ray photoelectron spectroscopy (XPS): The oxide layer on the heat treated sample was completely removed, but also in the case of the purely electropolished sample, the oxide layer was significantly reduced compared to the ''as received'' sample [26]. Correspondingly, for neither of the samples a processing could be observed, and E_{sat} was reached immediately.

The typical spot size development of Mo is presented in Fig. 10 and is visualized with SEM photographs shown in Table II. The full spot diameter of $\sim$1100 μm—an estimate based on an empirical fit of the form $\sim a[1-\exp(-x/b)]$—is achieved regardless of the sample preparation in about 40–50 sparks only, and is well in accordance with the value seen in Fig. 8(d). Note that, in some cases, already the first spark can leave traces that spread over the whole of the final damaged area, although these traces do not form a continuous spot of damage. This is due to the fact that the final spot diameter is determined by the geometry of the anode: Only the approximately flat, eroded part of the anode will create a high electric field region between the anode and the cathode, where initial field emission can take place. An anode with a larger diameter would create broader spots under the present experimental conditions.

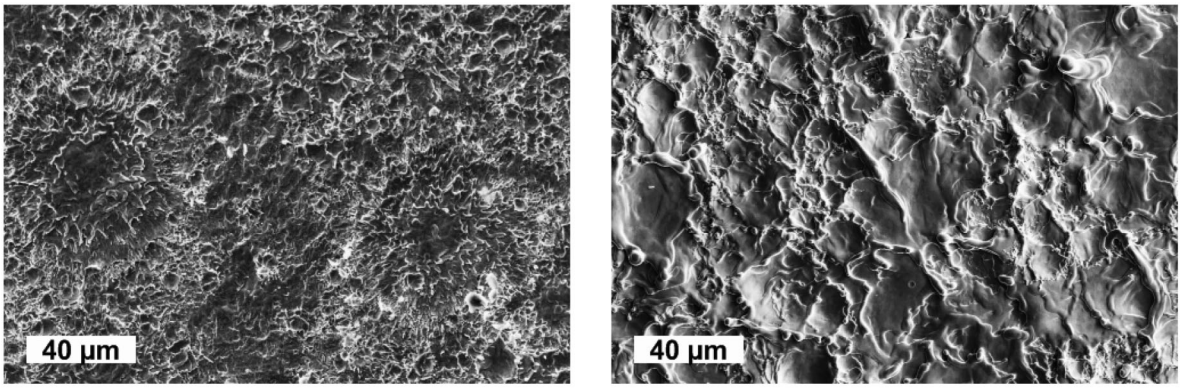

FIG. 9. SEM images of surface damage for Mo for low and high energy regimes. (a) Surface damage for $C_1 = 0.56$ nF (~ 10 mJ); the total number of sparks on the spot was 96. (b) Surface damage for $C_1 = 27.5$ nF (~ 850 mJ); the total number of sparks on the spot was 150.

To summarize our observations for Mo, we can state that (i) regardless of the surface treatment, the spot size grows during the typical processing phase of Mo and then saturates; at the same time, (ii) the oxide-free Mo does not exhibit processing, while the breakdown field of the oxidized Mo steadily grows as the spot size evolves. This might be because some unsparked, oxide covered areas are still present within the area of the final spot. When the oxide is removed from the entire spot area and the final spot size is reached, also the breakdown field saturates. Therefore, Mo conditions within 30–50 sparks. Thus, we propose a model for the DC processing.

IV. DISCUSSION

In this section, some peculiarities and limitations of the measurement system, the ''DC setup,'' and some of the results shall be discussed before final conclusions are drawn.

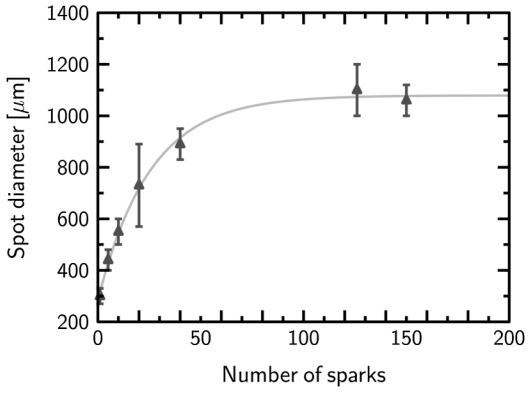

FIG. 10. Development of Mo spot size as a function of sparks; each point is an average over several measurements, all carried out with the standard capacitance, $C_1 = 27.5$ nF. The solid line is a least-squares fit of the form $\sim a[1 - \exp(-x/b)]$ to the data points x.

A. Energy range limitations

One matter of importance is to determine what is the lowest external capacitance C_1 providing reliable results. A rough order of magnitude estimate of the overall system stray capacitance gives about 0.1–1 nF. Therefore, additional experiments have been carried out with $C_1 = 0.1$ and 0.01 nF—corresponding to the order of 0.1–1 mJ—for both materials. In these cases, large oscillations originating from the system capacitance appeared on the discharge current signal and all measured breakdown properties (E_{sat}, β, E_{loc}) gave the same values as the measurements with $C_1 = 0.56$ nF. Both these facts assured us of where exactly the limitations in capacitance lay and that the measurements with $C_1 \geq 0.56$ nF give reliable results.

B. Measuring the field enhancement factor

In the Fowler-Nordheim equation [Eq. (1)], the field enhancement factor β was originally introduced as a constant, which is valid for any (j_{FE}, E_{ext}) in the range where the Fowler-Nordheim equation is applicable. In earlier experiments [14], however, we made the following observations on Cu: The repetitive application of an external electric field without producing breakdowns can (i) lead to a slow but steady growth of β if the electric field is high enough; also, (ii) it can lead to the decrease of β if the electric field is somewhat lower, e.g., through the ''relaxation'' of nanoscale surface features [27], through changes in the work function, etc. These results suggest that, in fact, β would not be a constant at all, but dynamically evolving, $\beta = \beta(E_{\mathrm{ext}})$. A possible explanation for this dependency is that surface charge would constantly redistribute through the repetitive application of E_{ext}, which in turn could facilitate the growth or relaxation of certain surface features.

In light of the above reasoning, if β were a function of E_{ext}, this would have two consequences for the measurements. First, since β is determined through the application

TABLE II. SEM photographs of the development of Mo spot size as a function of sparks on two samples with different surface treatments, both measured with $C_1 = 27.5$ nF. Note the different length scales in the pictures.

No. of sparks	Electropolished Mo	Electropolished, heat treated Mo
1	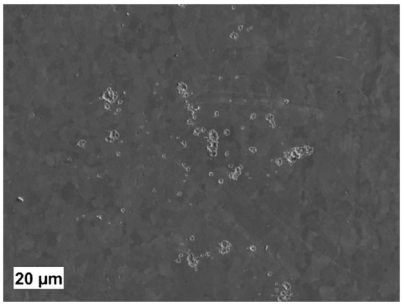	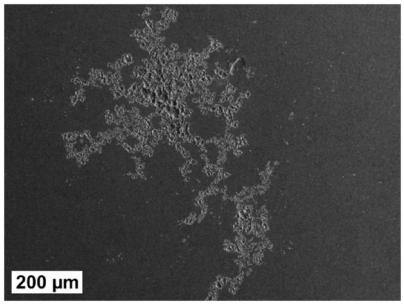
5	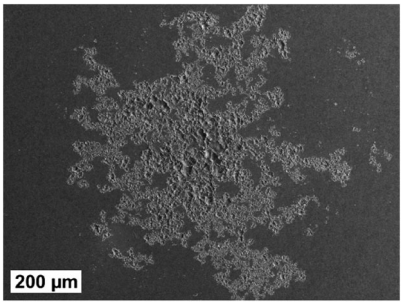	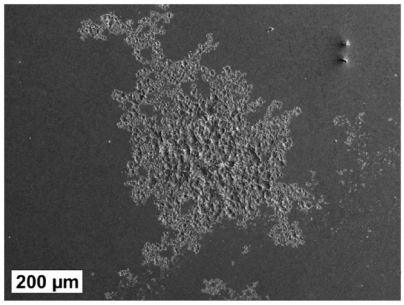
10	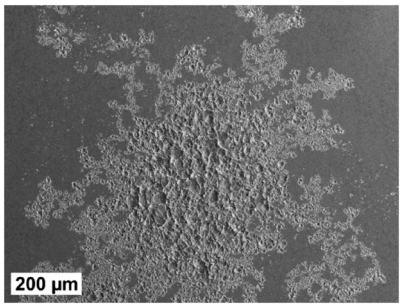	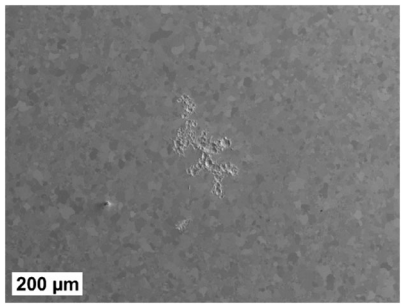
20	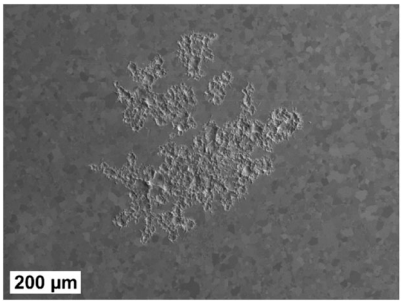	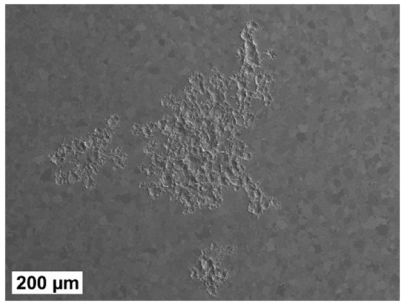
40	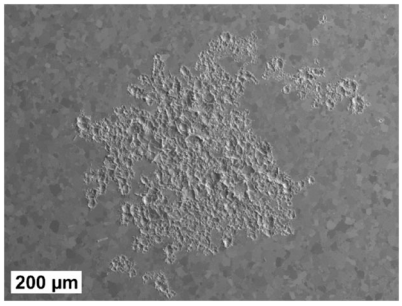	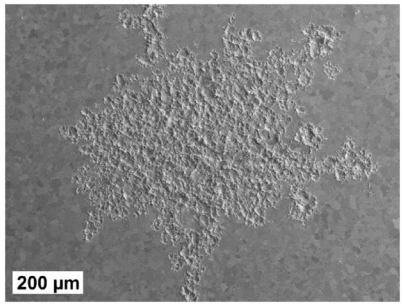

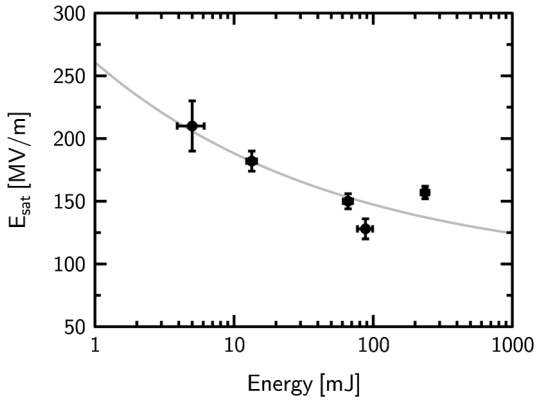

FIG. 11. Correlation between DC and rf energy dependency. The DC measurement points have been fitted to the behavior $E_{sat} \sim W^{-1/4}$ that is expected based on rf experiments.

of an electric field, the measurement itself could alter the outcome of the measurement. Second, the β measured may not necessarily be the same as the β at the moment the breakdown starts, since measurements of β and E_{sat} are carried out separately, with different electric field values and the voltage is even switched off in-between the two [28]. As often the primary interest in β and E_{loc} derived from it lays in the surveying of the conditions prevailing at the cathode at the moment of breakdown initiation, strictly speaking, these conditions are not accessible with the present experimental setup.

Finally, it should be pointed out that the change of C_1 (energy available) does not affect the electric circuit during β measurements (cf. Fig. 1). If we then argued that β does scale with energy for Cu (cf. Sec. III B 1), this dependency of β on energy could only be interpreted as a consequence of low and high energy breakdowns influencing the evolution of β in a different way. Several factors could play a role here: As measurements indicated, the surface can evolve differently (cf. Fig. 7), the efficiency of processing can be different (cf. Sec. III B 1), etc.

C. Energy scaling trends and their interpretation

To summarize the results obtained in Sec. III B, below we compare the energy scaling trends of Cu and Mo.

(i) The E_{sat} of Cu decreases with increasing energy by 40% over the energy range 5–90 mJ [Fig. 6(a)], while the E_{sat} of Mo increases by 38% over the range 10–850 mJ [Fig. 8(a)]. Both these trends have been attributed to the increasing efficiency of processing with more energy available for breakdown (cf. Sec. III C).

(ii) Concerning β and the E_{loc} associated with it, the trends for Cu and Mo differ. For Cu, β increases with increasing energy by 60% over the range 5–90 mJ [Fig. 6(b)], while E_{loc} remains constant within a relative overall variation of $\pm 13\%$ and a relative standard error of 6% [Fig. 6(c)]. For Mo, it is E_{loc} that increases by 26% over the range 10–1100 mJ [Fig. 8(c)], while β remains constant within a relative overall variation of $\pm 12\%$ and a relative standard error of 4% [Fig. 8(b)]. Why E_{loc} should be so stable for Cu while varying for Mo remains yet open; but given that E_{loc} determines the field emission prior to plasma buildup, the result suggests that the breakdown initiation mechanism may intrinsically be different for the two materials as a function of energy.

D. Correlation between DC and rf energy dependency

As a result of many years of Cu rf accelerating structure testing for linear colliders, the dependency of the accelerating gradient E on the pulse length τ at a constant breakdown probability was established to be $E \sim \tau^{-1/6}$ [7,8], as mentioned already in the Introduction. To see whether this dependency translates also to the DC case, we examined the scaling of E_{sat} for Cu [Fig. 6(a)] more carefully.

Since E_{sat} corresponds to a constant breakdown probability of about 10^{-2} [6], and assuming that the dependency observed in rf testing is valid also in DC experiments, we can state that $E \sim E_{sat} \sim \tau^{-1/6}$. Now just as in DC the energy available for breakdown W scales with both the capacitance C_1 and the charging voltage V as $W \sim C_1 V^2 \sim C_1 E_{sat}^2$, also in rf the energy stored in a pulse scales with both the pulse length τ and the voltage V as $W \sim \tau V^2 \sim \tau E^2$. Therefore the dependency $E \sim \tau^{-1/6}$ observed in rf translates to $E_{sat} \sim W^{-1/4}$ in DC, which is fitted to the data in Fig. 11. Although the presented rf scaling law describes the DC data well, we note that the DC data is insufficient to draw any conclusions on the exact exponent of the energy dependence of the Cu saturated field.

V. CONCLUSIONS

In the work presented, we have investigated how the processing and breakdown properties of Cu and Mo scale with the energy available for breakdown using energies in the range of about 5 to 240 mJ for Cu and about 10 to 1100 mJ for Mo. The electric field the material can sustain after processing (saturated field) is decreasing for Cu and increasing for Mo as a function of increasing energy. For Cu, the dependency of the local field causing field emission and the field enhancement factor on energy was very weak; the local field remained approximately constant with an average of (9.6 ± 0.4) GV/m. For Mo, the field enhancement factor remained constant at 34 ± 2 over the entire range investigated, and thus the local field showed the same trend as the saturated field. In the case of Cu, the constancy of the local field suggests that the local field might be an exclusively material dependent parameter characterizing how ''resistant'' the material is to breakdowns.

Concerning the processing properties of Mo, the processing speed was found to be depending on surface treatment, especially the surface oxide layer. For both

Cu and Mo, the processing speed was independent of energy. However, the energy dependence of the saturated field and Mo high energy preprocessing tests led to the conclusion that processing was more effective at higher energies. Furthermore, we have shown that the DC processing mechanism—at least for Mo—is related to surface oxide layer removal in the course of spot (damaged area) growth. As a consequence, processing speed appears to depend on the area of the surface damage caused by one breakdown, and is therefore affected by the spot growth speed and the surface treatment: No processing occurred when there was no oxide layer initially. On the other hand, the efficiency of processing depends on the depth of surface damage and how much oxide can be removed, which was suggested also by the analysis of the surface morphology of damaged areas processed at different energies.

[1] G. McCracken, J. Nucl. Mater. **93**, 3 (1980).

[2] D. Raboso, at the 6th International Workshop on Multipactor, Corona and Passive Intermodulation in Space RF Hardware (MULCOPIM '08), Valencia, Spain.

[3] W. Wuensch, in *Proceedings of the 8th European Particle Accelerator Conference, Paris, 2002* (EPS-IGA and CERN, Geneva, 2002), MOYGB003.

[4] H. H. Braun, S. Döbert, I. Wilson, and W. Wuensch, Phys. Rev. Lett. **90**, 224801 (2003).

[5] M. Kildemo, S. Calatroni, and M. Taborelli, Phys. Rev. ST Accel. Beams **7**, 092003 (2004).

[6] A. Descoeudres, T. Ramsvik, S. Calatroni, M. Taborelli, and W. Wuensch, Phys. Rev. ST Accel. Beams **12**, 032001 (2009).

[7] S. Doebert, C. Adolphsen, G. Bowden, D. Burke, J. Chan, V. Dolgashev, J. Frisch, K. Jobe, R. Jones, J. Lewandowski, R. Kirby, Z. Li, D. McCormick, R. Miller, C. Nantista, J. Nelson, C. Pearson, M. Ross, D. Schultz, T. Smith, S. Tantawi, J. Wang, T. Arkan, C. Boffo, H. Carter, I. Gonin, T. Khabiboulline, S. Mishra, G. Romanov, N. Solyak, Y. Funahashi, H. Hayano, N. Higashi, Y. Higashi, T. Higo, H. Kawamata, T. Kume, Y. Morozumi, K. Takata, T. Takatomi, N. Toge, K. Ueno, and Y. Watanabe, in *Proceedings of the 21st Particle Accelerator Conference, Knoxville, 2005* (IEEE, Piscataway, NJ, 2005), pp. 372–374.

[8] A. Grudiev, S. Calatroni, and W. Wuensch, Phys. Rev. ST Accel. Beams **12**, 102001 (2009).

[9] V. Dolgashev, S. Tantawi, Y. Higashi, and B. Spataro, Appl. Phys. Lett. **97**, 171501 (2010).

[10] C. E. Adolphsen, W. H. Baumgartner, R. K. Jobe, R. Loewen, D. McCormick, M. Ross, T. Smith, J. W. Wang, and T. Higo, Technical Report No. SLAC-PUB-8573, 2000.

[11] C. E. Adolphsen, W. H. Baumgartner, R. K. Jobe, F. Le Pimpec, R. Loewen, D. McCormick, M. Ross, T. Smith, J. W. Wang, and T. Higo, Technical Report No. SLAC-PUB-8901, 2001.

[12] V. A. Dolgashev and S. G. Tantawi, Technical Report No. SLAC-PUB-10175, 2003.

[13] M. Kildemo, Nucl. Instrum. Methods Phys. Res., Sect. A **530**, 596 (2004).

[14] A. Descoeudres, Y. Levinsen, S. Calatroni, M. Taborelli, and W. Wuensch, Phys. Rev. ST Accel. Beams **12**, 092001 (2009).

[15] R. H. Fowler and L. Nordheim, Proc. R. Soc. A **119**, 173 (1928).

[16] H. Padamsee, J. Knobloch, and T. Hays, *RF Superconductivity for Accelerators*, Wiley Series in Beam Physics and Accelerator Technology (Wiley, New York, 1998).

[17] R. Forbes, Ultramicroscopy **79**, 11 (1999).

[18] K. L. Jensen, Y. Y. Lau, D. W. Feldman, and P. G. O'Shea, Phys. Rev. ST Accel. Beams **11**, 081001 (2008).

[19] J. Hölzl, F. Schulte, and H. Wagner, *Solid Surface Physics, volume 85 of Springer Tracts in Modern Physics* (Springer, Berlin/Heidelberg, 1979).

[20] J. W. Wang and G. A. Loew, Stanford Linear Accelerator Center Report No. SLAC-PUB-7684, 1997.

[21] C. Scheuerlein and M. Taborelli, Appl. Surf. Sci. **252**, 4279 (2006).

[22] C. Crawford, J. Graber, T. Hays, J. Kirchgessner, A. Matheisen, W. D. Möller, H. Padamsee, M. Pekeler, P. Schmüser, and M. Tigner, Part. Accel. **49**, 1 (1995).

[23] H. Timko, K. Matyash, R. Schneider, F. Djurabekova, K. Nordlund, A. Hansen, A. Descoeudres, J. Kovermann, A. Grudiev, W. Wuensch, S. Calatroni, and M. Taborelli, Contrib. Plasma Phys. **51**, 5 (2011).

[24] C. Adolphsen, in Proceedings of the 21st Particle Accelerator Conference, Knoxville, 2005 (Ref. [7]), p. 204–208.

[25] T. Ramsvik, S. Calatroni, A. Reginelli, and M. Taborelli, Phys. Rev. ST Accel. Beams **10**, 042001 (2007).

[26] D. Letant-Delrieux, Technical Report No. EDMS 1035314, CERN, 2009 [https://edms.cern.ch/document/1035314/1].

[27] J. Frantz, M. Rusanen, K. Nordlund, and I. T. Koponen, J. Phys. Condens. Matter **16**, 2995 (2004).

[28] β is determined through measuring the electron field emission (FE) current as a function of the external field (cf. Fig. 1). Since there is a huge dynamic range between the FE current for β measurements ($\sim$ pA–nA) and the discharge current (10–100 A), these cannot be measured with the same device. Instead, β is measured first, then the voltage is switched off for a moment, and finally the voltage is ramped up until breakdown is reached to determine E_{sat}. In all cases, the typical voltage range used during β measurements was $\sim$1.5–2 kV. To determine E_{sat}, we used $\sim$6–8 kV for high energy Mo measurements, $\sim$4–6 kV for low energy Mo measurements, $\sim$2–3 kV for high energy Cu measurements, and $\sim$4–6 kV for low energy Cu measurements.